Diagn Interv Radiol 2021; 27: 654–663

INTERVENTIONAL RADIOLOGY

ORIGINAL ARTICLE

MRI and CT in the follow-up after irreversible electroporation of small renal masses

Mara Buijs
Daniel M. de Bruin
Peter G. K. Wagstaff
Patricia J. Zondervan
Matthijs J. V. Scheltema
Marc Engelbrecht
M. Pilar Laguna Pes
Krijn P. van Lienden

PURPOSE
Ablation plays a growing role in the treatment of small renal masses (SRMs) due to its nephron sparing properties and low invasiveness. Irreversible electroporation (IRE) has the potential, although still experimental, to overcome current limitations of thermal ablation. No prospective imaging studies exist of the ablation zone in the follow-up after renal IRE in humans. Objectives are to assess the use of computed tomography (CT) and magnetic resonance imaging (MRI) to determine the ablation zone volume (AZV), enhancement and imaging characteristics after renal IRE.

METHODS
This was a prospective phase 2 study of IRE in 9 patients with 10 SRMs. MRI was performed pre-IRE, 1 week, 3 months, 6 months, and 12 months after IRE. CT was performed pre-IRE, perioperatively (direct after ablation), 3 months, 6 months, and 12 months after IRE. AZVs were assessed by two independent observers. Observer variation was analyzed. Evolution of AZVs, and their relation with the needle configuration volume (NCV; indicating planned AZV) were evaluated based on CT and MRI measurements.

RESULTS
Eight SRMs were clear cell renal cell carcinomas, one SRM was a papillary renal cell carcinoma and one patient had a nondiagnostic biopsy. On CT, median AZV increased perioperatively until 3 months post-IRE (16.8 cm^3 and 6.2 cm^3, respectively) compared with the NCV (4.8 cm^3). On MRI, median AZV increased 1 week post-IRE until 3 months post-IRE (14.5 cm^3 and 4.6 cm^3, respectively) compared with the NCV (4.8 cm^3). At 6 months the AZV starts decreasing (CT 4.8 cm^3; MRI 3.0 cm^3), continuing at 12 months (CT 4.2 cm^3, MRI 1.1 cm^3). Strong correlation was demonstrated between the planned and the post-treatment volumes. Inter-observer agreement was excellent (CT: 95% CI 0.82–0.95; MRI: 95% CI 0.86–0.96). All SRMs appeared non-enhanced immediately after ablation, except for one residual tumor. Subtraction images confirmed non-enhancement on MRI in cases with unclear enhancement (3/9). Directly after IRE, gas bubbles, perinephric stranding, and edema were observed in all cases.

CONCLUSION
Both CT and MRI findings indicate increase of AZV until 3 months post-IRE, followed by gradual decrease in AZV from 6 to 12 months post-IRE. Enhancement is absent in cases with complete ablation. Gas bubbles, perinephric stranding, and edema are normal findings directly post-IRE.

From the Department of Urology (M.B. ✉ *m.buijs1@amsterdamumc.nl*, D.M.d.B., P.G.K.W., P.J.Z., M.J.V.S.), and Department of Radiology (M.W.E., K.P.v.L.), Department of Biomedical Engineering & Physics (D.M.d.B.), Academic Medical Center, Amsterdam, The Netherlands; Department of Urology (M.P.L.P.), Istanbul Medipol University, Istanbul.

Received 30 December 2019; revision requested 20 January 2020; last revision received 2 September 2020; accepted 29 September 2020.

Published online 20 August 2021.

DOI 10.5152/dir.2021.19575

Given the ageing population and increased incidental detection of small renal masses (≤4 cm, SRMs), focal therapies such as cryoablation and radiofrequency ablation gained interest due to their nephron-sparing properties and minimal invasiveness. A potential drawback of cryoablation and radiofrequency ablation is a lower efficacy in the proximity of vessels or the renal collecting system (heat sink effect) (1, 2). This may lead to an inadequate ablation and consequently residual- or recurrent disease (3). Additionally, vital structures (vessels, collecting system) can be damaged by the thermal process, causing necrosis and leading to perioperative or even long-term complications (4, 5). Irreversible electroporation (IRE), an electricity-based ablation modality, has the potential to circumvent these limitations as collagen structures, extracellular matrix and vital structures appear to be less affected compared with tumor tissue (6, 7).

You may cite this article as: Buijs M, de Bruin DM, Wagstaff PGK, et al. MRI and CT in the follow-up after irreversible electroporation of small renal masses. Diagn Interv Radiol 2021; 27: 654–663

Multiple studies have shown that renal IRE is safe and feasible (8–12). Except for one retrospective study with limited follow-up data (8), no previous study focused on the imaging characteristics and volume of the ablation zone (AZ) after renal IRE.

In pancreas, liver, and prostate, volume and ablation zone characteristics are investigated and described to guide the follow-up (13–15). Renal cell carcinoma (RCC) is very different from those tumors and comprises a wide variation of subtypes and inherently clinical behavior. Real-time image assessment using contrast-enhanced computed tomography (CT) is incorporated in renal ablation procedures to evaluate immediate technical success and to detect acute complications. It is yet unknown if the planned ablation size correlates with the definite ablation size in renal IRE, since it is an experimental ablation modality. Beside the two-dimensional, schematic needle-position that is created on the IRE generator at time of the ablation, no pre-treatment model exists that can predict the size and volume of the AZ. Currently, imaging in the follow-up is the only feedback on effectiveness of the ablation. In order to detect residual disease, early recurrence, and for planning and predicting the AZ, detailed knowledge on the imaging characteristics of post-treatment AZ and their evolution over time is vital. Therefore, the objective of this manuscript is to prospectively determine the IRE induced ablation zone volume (AZV) and its evolution over time using CT and magnetic resonance imaging (MRI). Second objective is to prospectively report on the imaging characteristics and enhancement of the IRE- induced AZ using CT and MRI.

Main points

- This study describes volume, enhancement and imaging characteristics over time after irreversible electroporation (IRE) of small renal masses in humans using CT and MRI.
- The ablation volume increases immediately after IRE, until 3 months after IRE. Subsequently a decrease of the volume occurs from 6 months until 12 months post-IRE.
- Enhancement on CT and MRI was absent post-IRE except for one residual tumor. Subtraction images may be useful to distinguish enhancement and predict residual disease or early recurrences.
- Directly after IRE, gas bubbles, perinephric stranding, and edema were observed on CT imaging.

Methods

Study design

This prospective, human, *in vivo*, IDEAL (idea, development, exploration, assessment, long-term study) phase 2 study is approved by the local Institutional Review Board (protocol decision number 2016_055). The study was executed according to the study protocol as previously reported (16). All patients gave written informed consent. Trial registration has been completed at the National Central Committee on Research Involving Human Subjects and in the clinicaltrials.gov database (NCT02828709).

Patients

Patients were consecutively included in the study and treated with percutaneous IRE between September 2016 and January 2018. Recruitment found place at the urology outpatient clinic. Inclusion criteria consisted of age ≥18 years, a solid, enhancing SRM on cross-sectional imaging suspicious for RCC, signed informed consent, and candidate for ablative therapy (16). Exclusion criteria were irreversible bleeding disorder, implantable cardioverter-defibrillator or pacemaker, severe cardiovascular disease, inability to stop anticoagulants (new oral anticoagulants or coumarin derivates) and inability for deep muscle relaxation and general anesthesia. The follow-up was 12 months. The indications for ablative therapy as well as the assessments on recurrence and residual diseases on post-IRE scans were evaluated in the multidisciplinary kidney board panel, consisting of interventional radiologists, urologists, nephrologists, and oncologists.

IRE procedure

As described in the study protocol (16), IRE ablation was performed using the IRE generator and associated needles (Nanoknife®, AngioDynamics) under general anesthesia with deep muscle relaxation (17). The procedure was performed at the interventional radiology department. Prior to the ablation, a renal mass biopsy was performed according to guidelines (18). IRE electrodes were placed percutaneously under CT guidance by an interventional radiologist experienced in IRE together with an urologist and a urology resident. The electrodes were positioned at the edge of the tumor. Maximum space between the needles was 2–2.4 cm. Three to six electrodes with an active tip exposure length of 15 mm to 20 mm, depending on the size of the tumor, were used to deliver the pulses. Immediately after the ablation a contrast-enhanced CT was performed to assess enhancement, volume and characteristics of the perioperative AZ.

Imaging follow-up schedule

Baseline CT and MRI were obtained from 1 day to 3 months prior to the ablation. MRI was performed at 1 week, 3 months, 6 months and 12 months post-IRE. CT was performed according to our institutional protocol for follow-up of renal mass ablation at 3 months, 6 months and 12 months post-IRE. As renal ablation patients receive substantial doses of ionizing radiation it was deemed unethical to perform additional CT scan at 1 week post-IRE.

Magnetic resonance imaging

A 1.5 Tesla AVANTO MRI scanner (Siemens Healthcare) with a surface phased, 16-channel body array matrix coil was utilized. A coronal T2-weighted localizing sequence was performed using fast imaging with balanced steady-state free precession (bSSFP) to confirm kidney location. Transverse diffusion-weighted images (b0, b500 s/mm^2; matrix 134×134; field of view (FOV) 380 mm; slice thickness 6 mm) were acquired. Breath-hold T2 weighted bSSFP transverse sequences with and without fat-suppression (matrix 384×230; FOV 350 mm; slice thickness 5 mm) were acquired, followed by single-shot breath-hold half-Fourier acquisition (HASTE) in coronal and transverse planes (matrix 320×256; FOV 400 mm; slice thickness 6 mm). Finally, breath-hold transverse unenhanced and contrast-enhanced T1-weighted three-dimensional transverse fat-suppressed spoiled gradient-echo images (matrix 320×240; FOV 400 mm; slice thickness 3 mm) were acquired before and at 0, 30, 60 and 90 s post arrival of contrast in the thoracic aorta. A coronal post-contrast plane was acquired at 90 s. For contrast enhancement, gadopentetate dimeglumine 0.2 mL/kg (Gd-DTPA) (Gadovist 1.0, Bayer Pharma; 0.1 mmol/kg of body weight) was administered at a rate of 2 mL/s using a power injector (Medrad) followed by a 20 mL saline flush.

Computed tomography

Scans were made on 384-slice CT scanner in supine position (SOMATOM Force, Siemens Healthcare). The renal tumor protocol

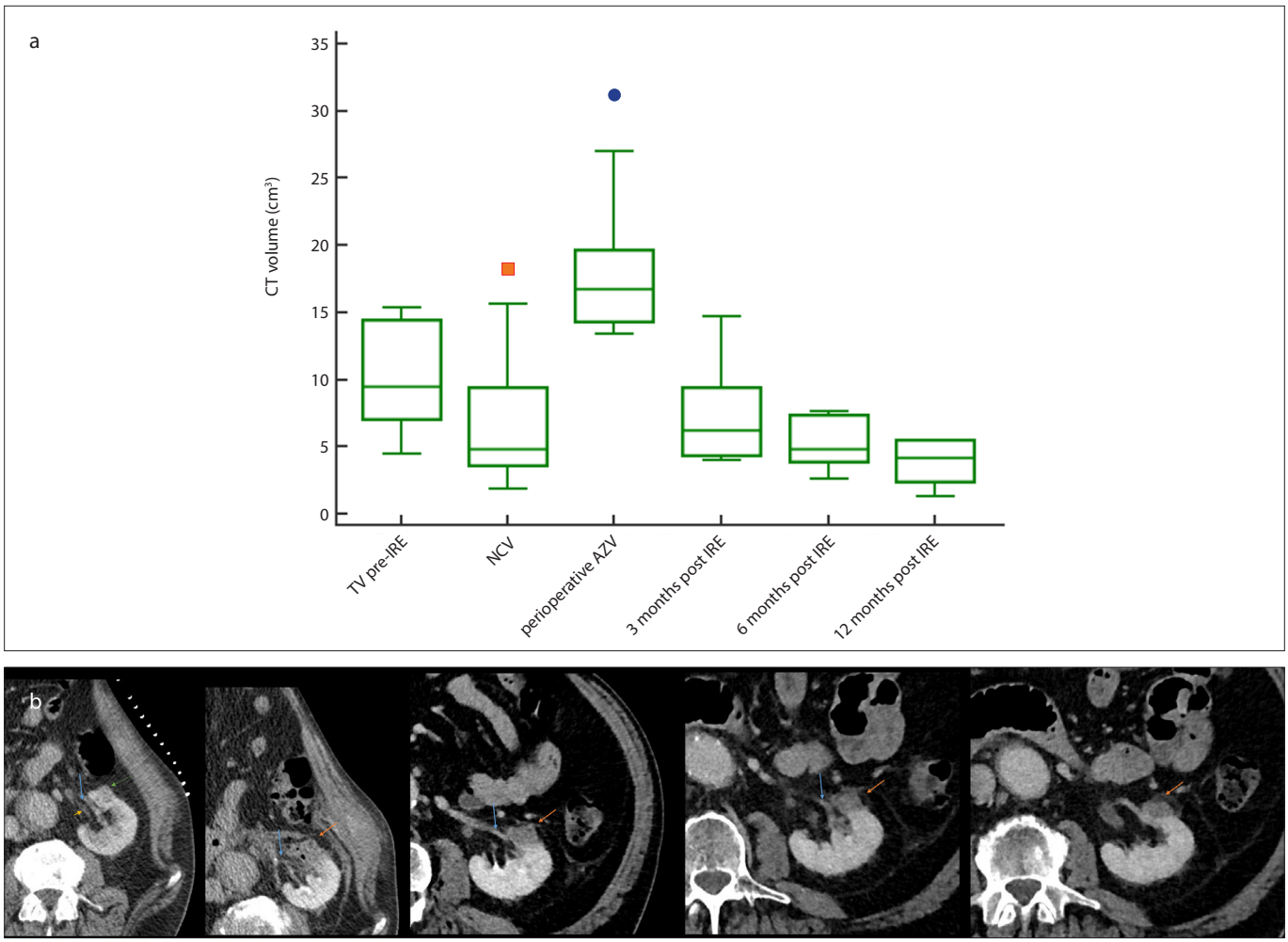

Figure 1. a, b. Panel **(a)** shows CT volumes in cm^3 over time (median, 25^{th}–75^{th} percentile). On x-axis from left to right: tumor volume (TV) pre-IRE (9.5 cm^3, 7.1–14.4 cm^3); needle configuration volume (NCV) (4.8 cm^3, 3.6–9.4 cm^3); perioperative ablation zone volume immediately after ablation (perioperative AZV) (16.8 cm^3, 14.3–19.6 cm^3); 3 months post-IRE AZV (6.2 cm^3, 4.4–9.4 cm^3); 6 months post-IRE AZV (4.8 cm^3, 3.9–7.4 cm^3); 12 months post-IRE AZV (4.2 cm^3, 2.5–5.5 cm^3). One outlier resembles SRM 7 with an initial tumor size of 3.9×3.9×3.7 cm. Panel **(b)** shows evolution of ablation zone through time as seen on CT. From left to right: tumor pre-IRE (4.5 cm^3); perioperative AZV (14.8 cm^3); 3 months post-IRE AZV (4.4 cm^3); 6 months post-IRE AZV (3.9 cm^3); 12 months post-IRE AZV (2.5 cm^3). Notice the proximity of the tumor pre-IRE *(green arrow)* and the ablation zone post-IRE *(orange arrow)* to the ureter *(yellow arrow)* and the renal vasculature in the hilum *(blue arrow)*.

consisted of a three-phase contrast-enhanced CT, with a slice thickness of 3 mm, after injection of 100 mL of contrast agent (Ultravist-300) with 4 mL/s to achieve enhancement. First, a pre-contrast scan was obtained. The arterial phase and corticomedullary phase were acquired after 45 s and 90 s respectively. Patients with an eGFR of 45–60 mL/min/1.73 m^2 were prehydrated according to our institutional protocol at the time.

Tumor and ablation zone volume

Volumes were measured using volume software (AGFA IMPAX Client 6.6.1.4024). The volumes were separately measured by two independent observers. The tumor volume (TV) and ablation zone volume (AZV) were measured by manual delineation of the lesion in the subsequent scan slices (19). The TV and the AZV were measured using the corticomedullary phase and in the dynamic series of CT and MRI respectively. The needle configuration volume (NCV) was defined as the volume between the active needle ends prior to the ablation. The cross-sectional surface between the IRE electrodes given by the software on the IRE console was multiplied by the active tip length (Supplementary Fig. 1). The perioperative AZV was defined as the AZV on contrast-enhanced CT performed at the end of the IRE procedure. The post-IRE AZV was defined as the AZV on cross-sectional imaging performed at 1 week (MRI only), 3 months (MRI and CT), 6 months (MRI and CT) and 12 months (MRI and CT) after IRE.

Imaging analysis

Characteristics were evaluated by an abdominal radiologist, an interventional radiologist and a resident urologist in consensus. On CT, characteristics of the AZ were evaluated. CT enhancement was measured by delineating a region of interest (ROI) within the tumor/post-IRE AZ. Density measurements were evaluated in Hounsfield units (HU). Lesion enhancement was calculated as follows: Three equally spaced CT slices were selected. In each slice a circular ROI was delineated within the AZ, excluding necrotic or cystic areas. The average HU value of all pixels within the three ROIs was calculated and used for analysis. On MRI, signal intensity and diffusion restriction (DR) were evaluated in post-contrast dynamic images, diffusion-weighted images (DWI), T2-weighted imaging, and non-contrast-en-

Table 1. Patient characteristics

	SRM 1	SRM 2	SRM 3	SRM 4	SRM 5	SRM 6	SRM 7	SRM 8	SRM 9	SRM 10
Patient characteristics										
Age (years)	72	60	68	66	60	60	77	77	70	73
Male	Y	Y	N	Y	Y	Y	N	N	Y	Y
Solitary kidney	N	Y	Y	Y	N	N	N	N	N	N
Serum creatinine (mg/dL)	88	194	85	144	77	82	70	82	122	112
Anticoagulant meds	Y*	Y*	N	Y	Y*	Y*	N	N	Y	N
Age-adjusted CCI	6	7	10	12	5	5	5	10	7	5

SRM 5 and 6 are respectively the right and left kidney of the same patient.
SRM, small renal mass; Y, yes; N, no; CCI, Charlson comorbidity index.
*Anticoagulant medication stopped before ablation and restarted after ablation.

Table 2. Tumor characteristics

SRM characteristics	SRM 1	SRM 2	SRM 3	SRM 4	SRM 5	SRM 6	SRM 7	SRM 8	SRM 9	SRM 10
Diameter (cm)	1.8	1.5	1.8	1.7	2.7	2.8	3.9	2.3	2	1.1
Dimensions (cm)	1.8x1.8x2.0	1.5x2.0x1.0	1.8x1.7x2.1	1.7x1.7x1.8	2.7x2.4x2.4	2.8x2.8x2.6	3.9x3.9x3.7	2.3x2.3x2.3	2x2.1x2.5	1.1x1.4x1.4
Side; Location pole	L; interpolar	R; lower	L; upper	R; interpolar	R; upper	L; lower	L; central	R; upper	L; lower	L; upper
A/P/X	A	P	P	A	P	P	P	P	A	X
PADUA	9	8	9	8	9	8	10	7	6	6
RENAL	7	6	6	5	8	6	8	5	5	4
Biopsy	ccRCC F2	ccRCC F2	ccRCC F3	ccRCC F2	pRCC T1 F1	ND	ccRCC F2	ccRCC F2	ccRCC F2	ccRCC F1
In proximity to vital structure	1 mm from calyx 12 mm from colon	5 mm from calyx	NA	NA	NA	5 mm from calyx	1 mm from spleen 1 mm from calyx	2 mm from liver 2 mm from calyx	5 mm from calyx	5 mm from colon
TNM	cT1aG2 cN0cM0	cT1aG2 cN0cM0	cT1aG3 pN1pM1	cT1aG2 cN0pM1	cT1aG1 cN0cM0	cT1aGx cN0cM0	cT1aGx cN0cM0	cT1aG2 cN0cM0	cT1aG2 cN0cM0	cT1aG1 cN0cM0

SRM 5 and 6 are respectively the right and left kidney of the same patient.
SRM, small renal mass; L, left; R, right; A, anterior; P, posterior; PADUA, Preoperative Aspects and Dimensions Used for an Anatomical classification; RENAL score, Radius (tumor size as maximal diameter), Exophytic/endophytic properties of the tumor, Nearness of tumor deepest portion to the collecting system or sinus, Anterior (a)/posterior (p) descriptor and the Location relative to the polar line; ccRCC, clear cell renal cell carcinoma; pRCC, papillary renal cell carcinoma; ND, nondiagnostic biopsy; TNM, tumor node metastasis score; NA, not applicable.

hanced sequences. To confirm enhancement subtraction images were made.

Statistical analysis

For both CT and MRI volumes, inter-observer reliability was assessed using the intra-class coefficient (ICC). ICC estimates and their 95% confidence intervals (CIs) were calculated based on mean-rating (k=2), consistency, and two-way random-effects model, according to McGraw and Wong (20). The 95% CI of the ICC estimate guided the interpretation (21): values below 0.5 were interpreted as poor reliability, between 0.5 and 0.75 as moderate reliability, between 0.75 and 0.9 as good reliability, and values greater than 0.90 as excellent reliability. Both raters were blinded to each other's results. The volume and enhancement measurements were expressed as medians and interquartile range (IQR) since the data were not normally distributed. Comparison of the volume on CT with the volume on MRI per time point was illustrated using Bland-Altman plots. The relation between the planned volumes (NCV), and the CT-AZVs and MRI-AZVs was analyzed using scatterplots. Statistical analyses were performed using MedCalc Statistical Software for mac, version 15.8 (MedCalc Software).

This imaging study is part of a safety and feasibility pilot study (16). For the aim of this study, evaluation of ten IRE-treated SRMs were required.

Results

Nine patients with ten SRMs with a median age of 68 years (IQR 60–77 years) were treated and included. Patient and tumor characteristics are summarized in Tables 1 and 2. Two patients had chronically impaired renal function preoperatively (stage 3B). Three patients had a solitary kidney. The follow-up was 12 months in all patients, except for one patient in whom residual tumor was diagnosed at 3 months. This patient (SRM 7) underwent salvage cryoablation and was therefore excluded from follow-up after 6 months. One patient had a nondiagnostic biopsy during ablation (SRM 6). One patient was diagnosed with bilateral tumors and underwent bilateral IRE ab-

Table 3. Comparison of volumes between timepoints	
Timepoint	Median (IQR) in cm^3
CT tumor volume (TV)	9.5 (7.1–14.4)
Needle configuration volume (NCV)	4.8 (3.6–9.4)
CT perioperative ablation zone volume (peri-AZV)	16.8 (14.3–19.6)
CT 3 months post-IRE ablation zone volume (3-AZV)	6.2 (4.4–9.4)
CT 6 months post-IRE ablation zone volume (6-AZV)	4.8 (3.9–7.4)
CT 12 months post-IRE ablation zone volume (12-AZV)	4.2 (2.2–5.5)
MRI tumor volume (TV)	7.1 (2.6–11.4)
Needle configuration volume (NCV)	4.8 (3.6–9.4)
MRI 1 week post-IRE ablation zone volume (1w-AZV)	14.5 (12.0–30.4)
MRI 3 months post-IRE ablation zone volume (3-AZV)	4.6 (2.6–12.8)
MRI 6 months post-IRE ablation zone volume (6-AZV)	3.0 (1.5–6.8)
MRI 12 months post-IRE ablation zone volume (12-AZV)	1.1 (0.9–4.5)

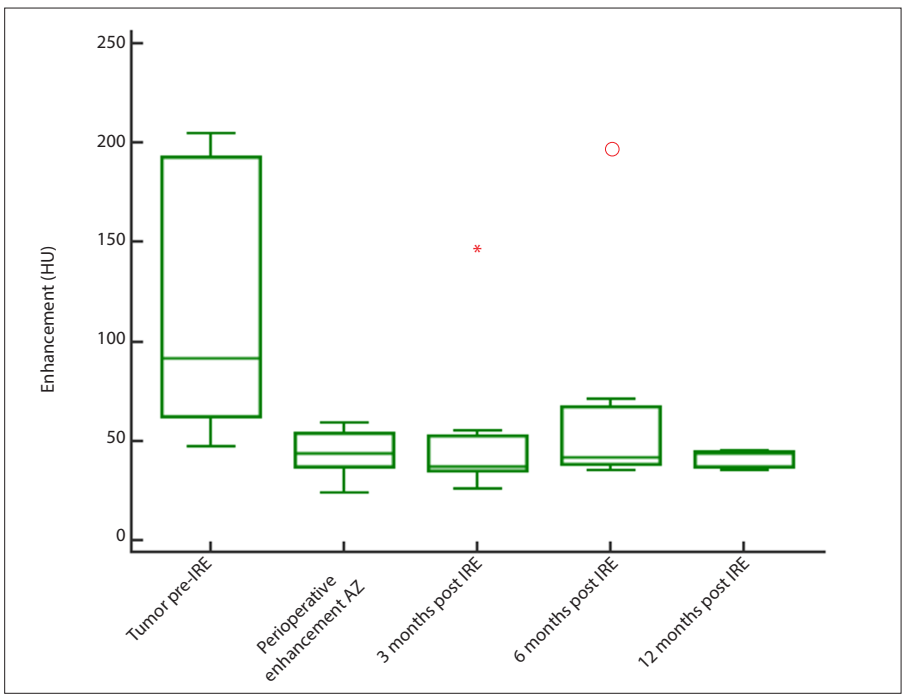

Figure 2. CT enhancement in Hounsfield Units (HU) over time (median, 25th–75th percentile). On x-axis from left to right: tumor enhancement pre-IRE (92 HU, 62–193 HU); perioperative enhancement of ablation zone immediately after ablation (perioperative enhancement) (44 HU, 37–54 HU); 3 months post-IRE enhancement (37 HU, 35–52 HU); 6 months post-IRE enhancement (42 HU, 39–67 HU); 12 months post-IRE enhancement (44 HU, 37–45 HU). The outlier at 3 months post-IRE and 6 months post-IRE is the residual tumor of SRM 7.

lation in two separate sessions (SRM 5 and SRM 6). One patient was unable to undergo MRI due to claustrophobia. One pre-IRE MRI was missing since the patient was referred from another hospital.

For CT evaluation of IRE, ICC was 0.91 (95% CI 0.82–0.95). The median tumor volume (TV) on CT was 9.5 cm^3 (7.1–14.4 cm^3). The median NCV was 4.8 cm^3 (3.6–9.4 cm^3). The median perioperative AZV (immediately after ablation) was 16.8 cm^3 (14.3–19.6 cm^3) and 3.5 times larger compared to the NCV. At 3 months post-IRE the median AZV was 6.2 cm^3 (4.4–9.4 cm^3). At 6 months and 12 months the median AZV was 4.8 cm^3 (3.9–7.4 cm^3), and 4.2 cm^3 (2.5–5.5 cm^3), respectively. Volume outcomes are described in Fig. 1 and Table 3, respectively.

Pre-IRE, median tumor enhancement was 92 HU (62–193 HU). The perioperative AZ showed a median decrease in enhancement to 44 HU (37–54 HU). At 3 months post-IRE, the median AZ enhancement was 37 HU (35–52 HU), at 6 months post-IRE the median AZ enhancement was 42 HU (39–67 HU) and at 12 months was 44 HU (37–45 HU). Enhancement data are depicted in Fig. 2.

In the perioperative AZ we observed "gas bubbles" in proximity of, and within, the ablation zone in all cases (10/10) (Fig. 3). On the contrast-enhanced, perioperative CT scan performed directly after ablation, there was clearly an ablated tumor visible, which could be distinguished from the edema/inflammation surrounding the ablated tumor in majority of cases (6/10) (Fig. 4). Perinephric stranding developed immediately after ablation which persisted and gradually reduced during the 12-month follow-up (10/10) (Figs. 3 and 4).

For MRI evaluation of IRE, ICC was 0.92 (95% CI, 0.86–0.96). The median TV pre-IRE was 7.1 cm^3 (2.6–11.4 cm^3) on MRI. The median NCV was 4.8 cm^3 (3.6–9.4 cm^3). The median volume post-IRE at 1 week was 14.5 cm^3 (12.0–30.4 cm^3) and 3 times larger when compared with the NCV. At 3 months post-IRE the median volume was 4.6 cm^3 (2.6–12.8 cm^3), at 6 months post-IRE 3.0 cm^3 (1.5–6.8 cm^3), and at 12 months post-IRE 1.1 cm^3 (0.9–4.5 cm^3). Volume outcomes are described in Fig. 5 and Table 3, respectively.

On pre-IRE imaging, 7 SRMs showed enhancement in the arterial phase on T1volumetric interpolated breath-hold examination (VIBE), which was confirmed by subtraction images (7/8). Three SRMs showed presence of focal DR (3/8). For the non-contrast-enhanced phase, 4 SRMs were isointense, 2 SRMs were hypointense, and 2 SRMs were hyperintense. At T2-weighted imaging, 2 SRMs were isointense, 3 SRMs were hypointense, 3 SRMs were hyperintense.

After ablation, most AZs developed hyperintensity on non-contrast-enhanced phase through the follow-up of 12 months (6/9). Other AZs developed hyperintensity but resolved after 1 week to 3 months and became isointense (3/9).

On T1 VIBE sequence, all AZs were non-enhanced post-IRE, with the exception of the residual tumor. Eight SRMs showed non-enhancement 1 week after ablation in the arterial phase and remained like this until the end of the study (8/9). Subtraction images confirmed the non-enhancement in all 9 SRMs. One SRM contained residual tumor (SRM 7) (1/9) showing heterogeneous

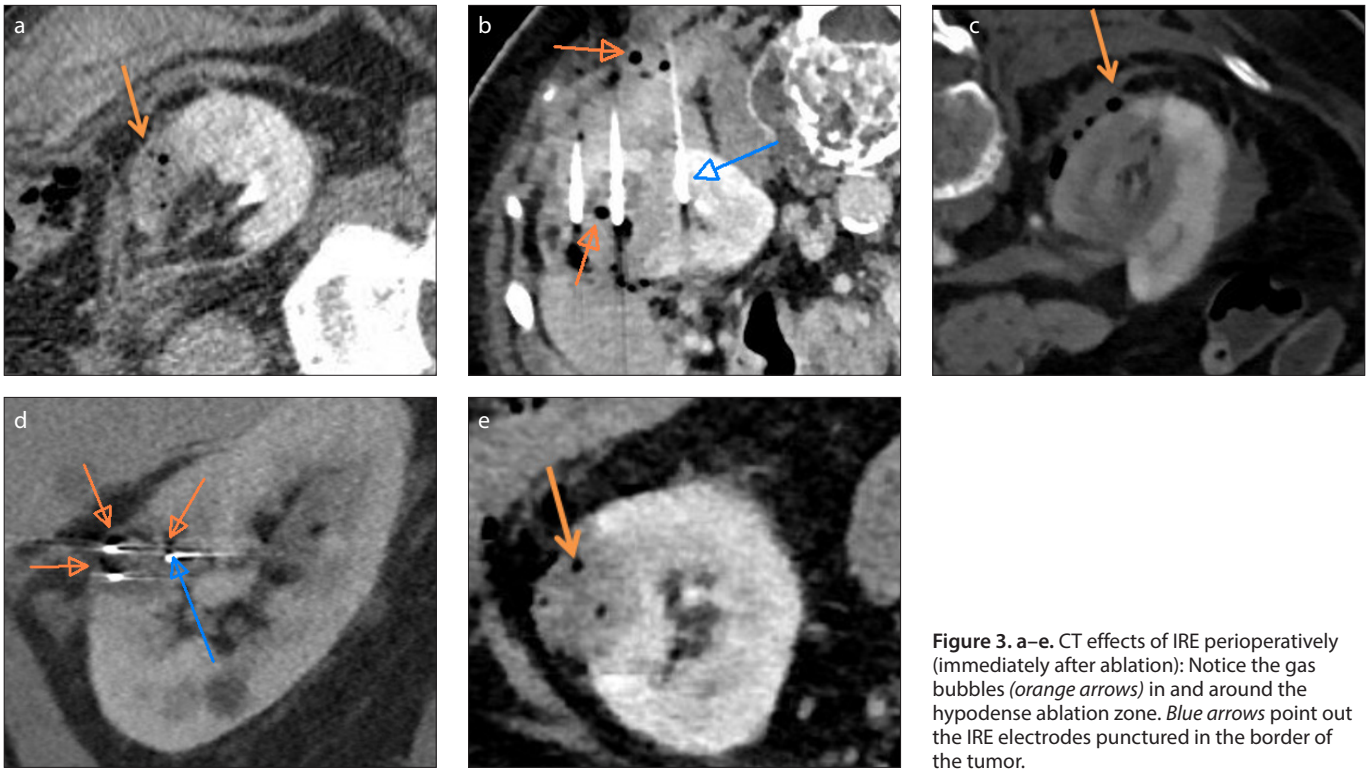

Figure 3. a–e. CT effects of IRE perioperatively (immediately after ablation): Notice the gas bubbles *(orange arrows)* in and around the hypodense ablation zone. *Blue arrows* point out the IRE electrodes punctured in the border of the tumor.

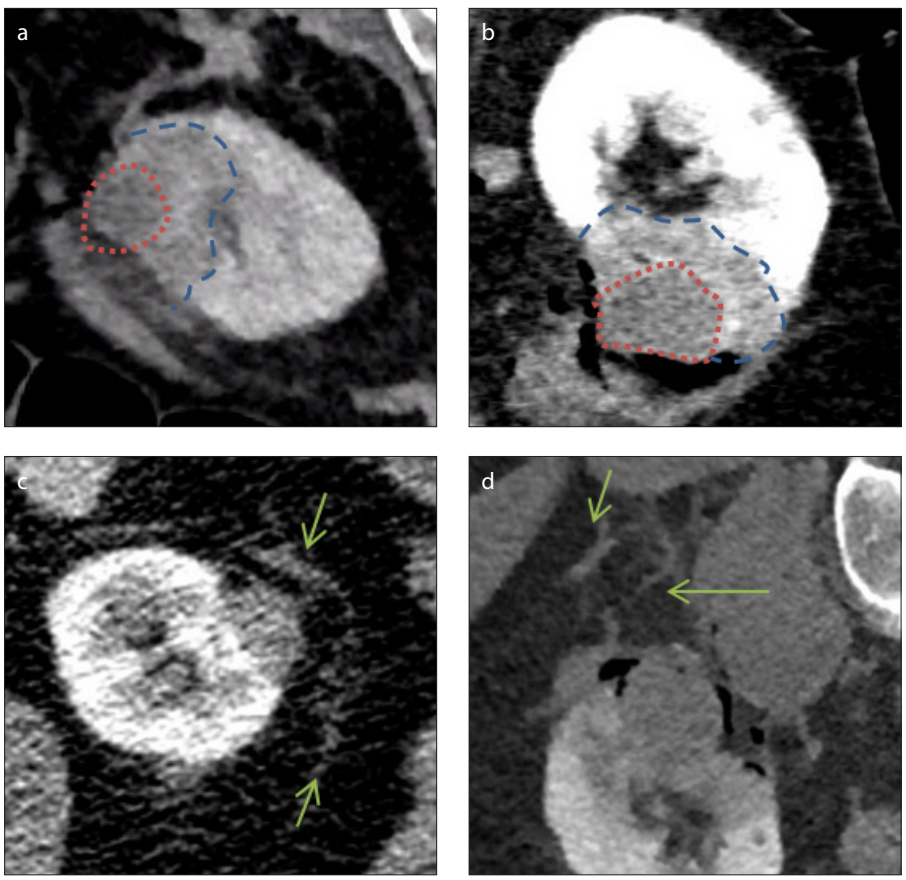

Figure 4. a–d. CT effects of IRE perioperatively. Panels **(a, b)** show CT scan performed perioperatively in SRM 10 and 6, respectively. *Red lining* indicates the hypodense ablated tumor. *Blue lining* indicates the edematous and inflammation tissue surrounding it, also hypodense but less grey. Panel **(c)** shows CT scan performed 3 months post-IRE in SRM 8. *Green arrows* indicate the perinephric stranding. Panel **(d)** shows CT scan performed perioperatively in SRM 5. *Green arrows* outlining the perinephric stranding.

signal at 1 week and persisting enhancement from 3 months on.

On diffusion-weighted images, majority of the SRMs showed no presence of focal DR post-IRE. In the minority of cases presence of focal DR was seen at one time point but was transient. In 7 of 9 SRMs there was no DR during the entire follow-up of 1 year post-IRE. In 3 SRMs, there was presence of focal DR at 1 week and at 3 months but resolved after this follow-up visit.

On T2-weighted imaging, the majority of masses were hypointense after ablation (7/9). In the minority there was heterogeneous signal, which evolved to hypointensity in time (2/9).

The scatterplots of MRI and CT plotted against the NCV showed a strong correlation for both CT and MRI, with larger intercepts for CT than for MRI at every time point (Fig. 6). Bland-Altman plots of CT and MRI per time point showed a mean difference (estimated bias) of -0.7 cm^3 for the tumor volume prior to ablation, -0.7 cm^3 at 3 months post-IRE, -0.18 cm^3 at 6 months post-IRE and 0.52 cm^3 at 12 months post-IRE (Fig. 7).

Discussion

This prospective study assessed MRI and CT findings pre- and post-IRE treatment for SRMs. There was no loss to follow-up and the follow-up visits were planned

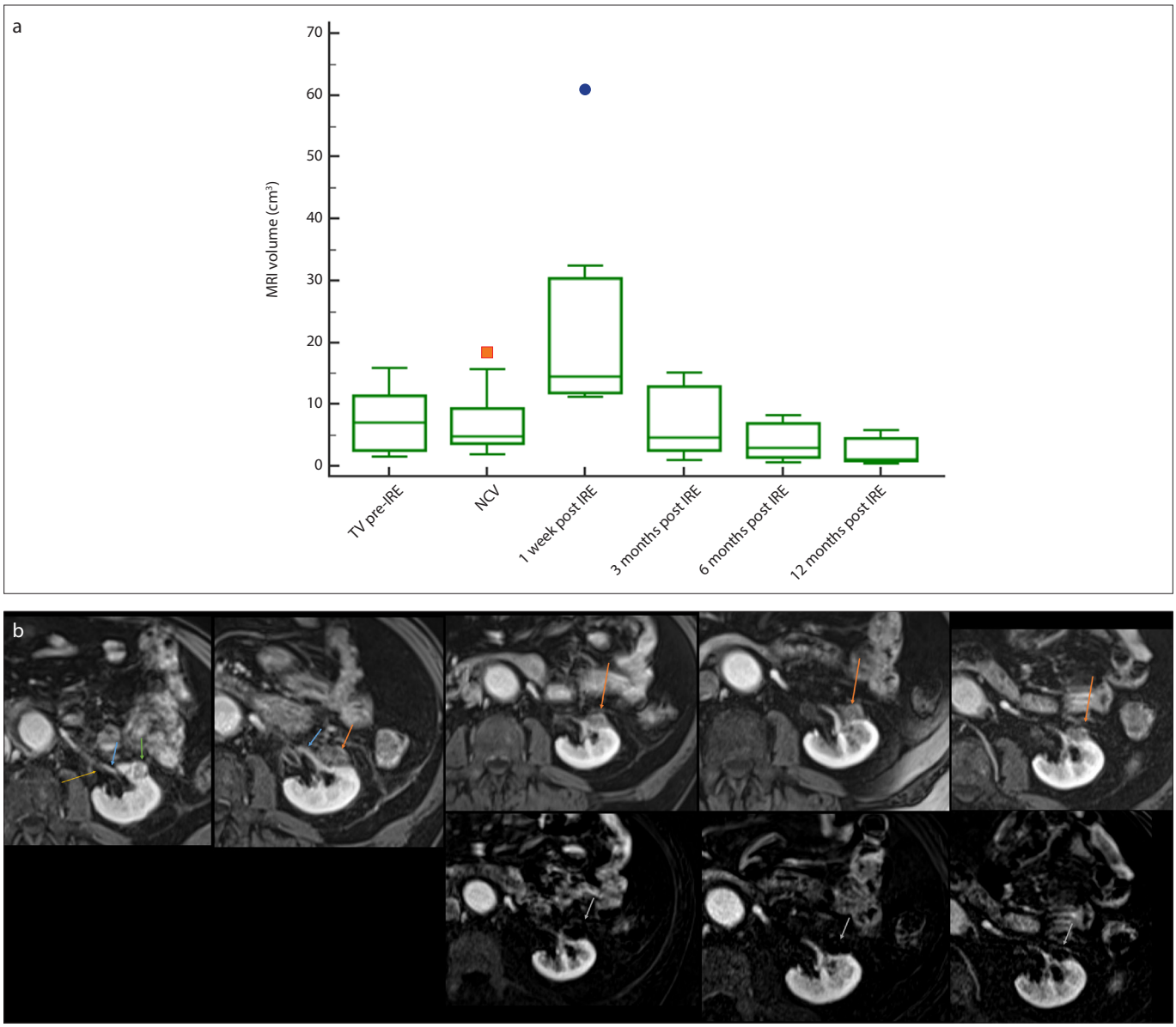

Figure 5. a, b. Panel **(a)** shows MRI volumes in cm^3 over time (median, 25th–75th percentile). On x-axis from left to right: tumor volume (TV) pre-IRE (7.1 cm^3, 2.6–11.4 cm^3); needle configuration volume (NCV) (4.8 cm^3, 3.6–9.4 cm^3); 1 week post-IRE volume (14.5 cm^3, 12.0–30.4 cm^3; 3 months post-IRE (4.6 cm^3, 2.6–12.8 cm^3); 6 months post-IRE (3.0 cm^3, 1.5–6.8 cm^3); 12 months post-IRE (1.1 cm^3, 0.9–4.5 cm^3). One outlier resembles SRM 7 with an initial tumor size of 3.9×3.9×3.7 cm and was the residual tumor diagnosed at 3 months. Panel **(b)** shows evolution of ablation zone through time on MRI. From left to right: tumor pre-IRE (PA: clear cell RCC, 3.4 cm^3); 1 week post-IRE (11.3 cm^3); 3 months post-IRE (4.3 cm^3); 6 months post-IRE (3.6 cm^3); 12 months post-IRE (1.3 cm^3). Notice the proximity of the tumor pre-IRE *(green arrow)* and the ablation zone post-IRE *(orange arrow)* to the ureter *(yellow arrow)* and the renal vasculature in the hilum *(blue arrow)*. See subtraction images below to clarify possible enhancement of ablation zone seen on post-contrast dynamic images (upper row).

according to regularly scheduled time-points, as in clinical practice. Expertise on pre- and post-IRE MRI and CT images is an unmet need for planning renal IRE ablation, and for determination of the ablation response and treatment effect (20). We reported an increase of the AZV on respectively CT and MRI immediately after ablation until 1 week post-IRE and 3 months post-IRE. At 6 months, the AZV started to decrease in comparison to the perioperative AZV, 1 week and 3 months post-IRE. This decrease continued until the end of the study at 12 months. The increase of the ablation zone can be clarified by possible edema, reactive inflammation tissue and transient hyperemia. The increase is consistent with previous articles: Trimmer et al. (8) reported this increase in a retrospective patient series. Other research demonstrated an increase and subsequently a decrease of lesion size after renal ablation, although these observations were in pigs (21, 22). In other organs, such as pancreas and prostate, ablation zone was investigated and similarly reported the increase (13, 14).

All SRMs appeared non-enhanced 1 week after ablation until the end of the study on MRI and CT, except for one patient with a residual tumor. In case of unclear tumor enhancement (3/9), subtraction images were especially helpful confirming non-enhancement (Fig. 5b). One patient (SRM 7) had a residual tumor, diagnosed at 3 months post-IRE and biopsy confirmed (clear cell renal cell carcinoma Fuhrman grade 3). This

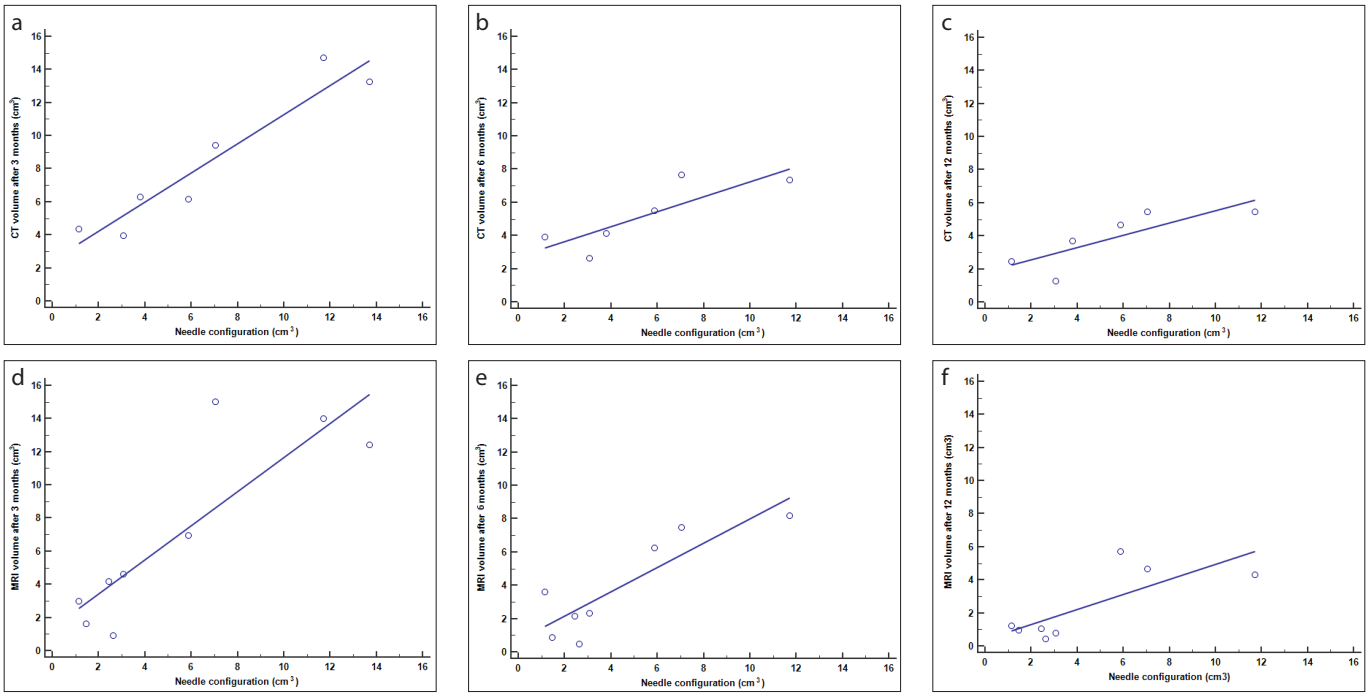

Figure 6. a–f. Scatterplots of CT volumes correlated with the needle configuration volume (NCV) at 3 months (**a**), 6 months (**b**), and 12 months (**c**) post-IRE; scatterplots of MRI volumes correlated with the NCV at 3 months (**d**), 6 months (**e**), and 12 months (**f**) post-IRE.

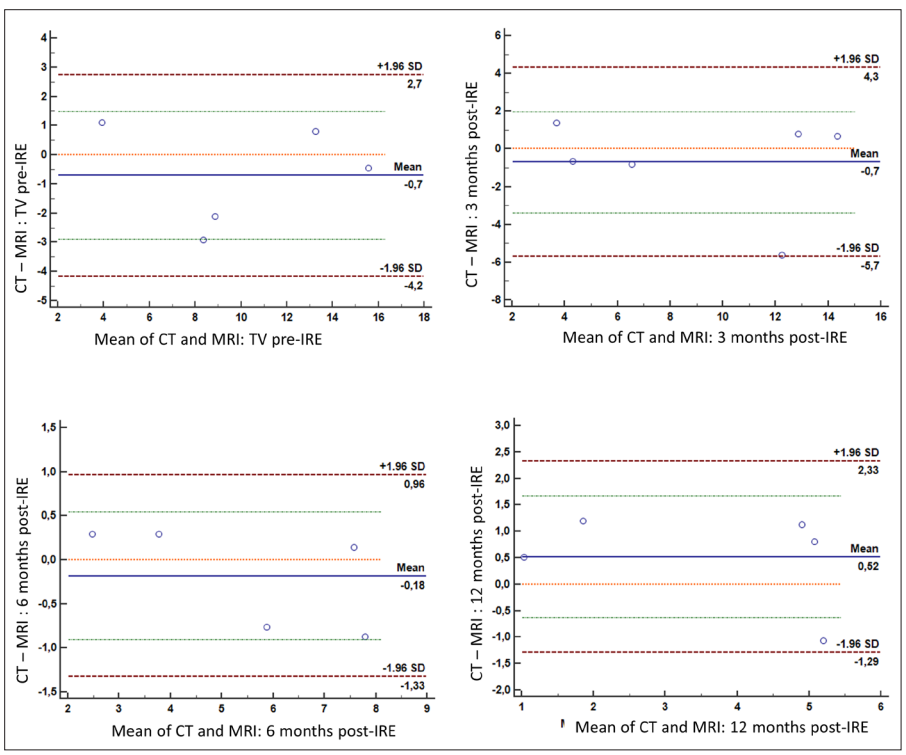

Figure 7. Bland-Altman plot per time point of CT vs. MRI. From left to right: A mean difference (estimated bias) of -0.7 cm^3 of the tumor volume prior to ablation, -0.7 cm^3 at 3 months post-IRE, -0.18 cm^3 at 6 months post-IRE, and 0.52 cm^3 at 12 months post-IRE.

patient resembles an outlier for the volumes and for the enhancement post-IRE. The tumor size was 3.9×3.9×3.7 cm, hence this was the largest in our cohort. Literature has shown that tumors of 4 cm or larger decreases the effectiveness of IRE (23), emphasizing that we should be cautious in future with ablating large tumors. Several other MRI sequences, such as the non-contrast-enhanced, diffusion weighted images, and T2-weighted images, were analyzed but did not appear to have an additional clinical use. Obviously, the sample size of our pilot study is small, therefore these conclusions should be interpreted with caution.

We attempted to compare CT with MRI to evaluate if both imaging techniques deviate from each other and therefore may be more suitable for IRE follow-up. The Bland-Altman plots demonstrated that after renal IRE the MRI volumes were slightly larger than the CT volumes. The relation between the NCV (the planned volume) and the post-treatment volumes demonstrated a strong correlation. According to these analyses, CT volumes were slightly larger than MRI volumes. Again, our sample size is small hence reliable conclusions are not yet to be drawn based on this cohort. When looking at the evaluation of visual characteristics after renal IRE, MRI had an advantage over CT. When there were doubts about recurrences or residual tumor due to unclear enhancement, which is often the case after ablation due to reactive edema or inflammation tissue, the subtraction images of MRI were able to differentiate between the latter.

On both MRI and CT, the TV appears larger than the NCV. Based on previous experiments in porcine kidney, we assumed that the eventual ablation zone exceeds the NCV with approximately 5 mm in every direction (24). This has never been properly

investigated for renal IRE in humans, hence those calculations were not considered for our NCV. However, in prostatic IRE studies in humans this has been confirmed with histopathology correlation (13).

Although we had a vulnerable study population including 3 solitary kidneys, IRE was well-tolerated. Two patients had grade 3 adverse event according to the Common Terminology Criteria for Adverse Events (CTCAE). One patient with a solitary kidney experienced pain and had impaired renal function due to a blood clot which partially obstructed the ureter postoperative. After a double J ureteral stent was inserted his renal function returned to preoperative levels (CTCAE grade 3). One patient had pyelonephritis 17 days after the ablation requiring admission for two days and IV antibiotics (CTCAE grade 3). Three patients had CTCAE grade 1 adverse event (macroscopic hematuria, painful micturition, perinephric hematoma). The renal functions of all patients returned to pre-operative levels. All patients recovered from their minor or major complication without any lasting symptoms.

Our study is limited by a small sample size as the primary objective of the study was to assess technical feasibility and safety. The second objective was to evaluate the use of several imaging modalities, including CT and MRI, on the visualization of the ablation zone in the follow-up after renal IRE. For determining AZVs in imaging after IRE, several studies have demonstrated that correlation is excellent in a small number of cases (13, 25). Another limitation is the comparison of multiple types of NCVs (2–6 needle configurations). For uniformity of the ablation zones, ideally the same number of needles should be used in every patient. As IRE was used as a curative treatment in our trial and differently sized tumors were included, it was considered unethical to use the same NCV for every tumor. At last, our study is limited by a lack of histopathologic confirmation during follow-up. Generally, guidelines recommend renal mass biopsies only in case of suspicion on cross-sectional imaging (18). Ideally, optimal correlation of CT and MRI with histopathology would have required a nephrectomy. Considering that this population was extremely vulnerable, we decided not to obtain histopathology. In this study, we have quantified the ablation zone post-IRE in SRMs. With this, we are providing a foundation for larger trials to further investigate follow-up imaging after renal IRE, and providing guidance to clinicians for planning IRE ablation and monitoring response.

In conclusion, the AZV increases after renal IRE ablation. At 6 months the decrease of the AZV starts gradually until 12 months. Enhancement was absent post-IRE, except for one patient showing residual tumor. On MRI, subtraction images can be used to confirm non-enhancement accurately and hence may be applied as a predictor for residual disease or early recurrences. Gas bubbles, perinephric stranding and edema are normal findings on CT and MRI directly after renal IRE.

Financial disclosure

This study is supported and funded by ZonMW. All data will be published in international peer-reviewed medical journals and presented at international conferences. The funding bodies have posed no publication restrictions.

Conflict of interest disclosure

The authors declared no conflicts of interest.

References

1. Pillai K, Akhter J, Chua TC, et al. Heat sink effect on tumor ablation characteristics as observed in monopolar radiofrequency, bipolar radiofrequency, and microwave, using ex vivo calf liver model. Medicine 2015; 94:e580. [Crossref]
2. Chu KF, Dupuy DE. Thermal ablation of tumours: biological mechanisms and advances in therapy. Nature Reviews Cancer 2014; 14:199–208. [Crossref]
3. Ringe KI, Lutat C, Rieder C, Schenk A, Wacker F, Raatschen HJ. Experimental evaluation of the heat sink effect in hepatic microwave ablation. PLoS One 2015; 10:e0134301. [Crossref]
4. Park BK, Kim CK. Complications of image-guided radiofrequency ablation of renal cell carcinoma: Causes, imaging features and prevention methods. Eur Radiol 2009; 19:2180–2190. [Crossref]
5. Gervais DA, Arellano RS, McGovern FJ, McDougal WS, Mueller PR. Radiofrequency ablation of renal cell carcinoma: part 2, Lessons learned with ablation of 100 tumors. AJR Am J Roentgenol 2005; 185:72–80. [Crossref]
6. Wendler JJ, Pech M, Friebe B, et al. Upper-urinary-tract effects after irreversible electroporation (IRE) of human localised renal-cell carcinoma (RCC) in the IRENE pilot phase 2a ablate-and-resect study. Cardiovasc Interv Radiol 2017; 41:466–476. [Crossref]
7. Rubinsky B, Onik G, Mikus P. Irreversible electroporation: A new ablation modality - Clinical implications. Technol Cancer Res Treat 2007; 6:37–48. [Crossref]
8. Trimmer CK, Khosla A, Morgan M, Stephenson SL, Ozayar A, Cadeddu JA. Minimally invasive percutaneous treatment of small renal tumors with irreversible electroporation: a single-center experience. J Vasc Interv Radiol 2015; 26:1465–1471. [Crossref]
9. Tracy CR, Kabbani W, Cadeddu JA. Irreversible electroporation (IRE): A novel method for renal tissue ablation. BJU Int 2011; 107:1982–1987. [Crossref]
10. Thomson KR, Cheung W, Ellis SJ, et al. Investigation of the safety of irreversible electroporation in humans. J Vasc Interv Radiol 2011; 22:611–621. [Crossref]
11. Wendler JJ, Ricke J, Pech M, et al. Initial assessment of clinical feasibility, safety and efficacy of NanoKnife irreversible electroporation (IRE) in the focal treatment of localized renal cell carcinoma (RCC) with delayed interval tumor resection (IRENE trial). Eur Urol Suppl 2017; 16:e102–e103. [Crossref]
12. Buijs M, Zondervan PJ, de Bruin DM, van Lienden KP, Bex A, van Delden OM. Feasibility and safety of irreversible electroporation (IRE) in patients with small renal masses: Results of a prospective study. Urol Oncol Semin Orig Investig 2019; 37:183.e1–183.e8. [Crossref]
13. van Den Bos W, de Bruin DM, van Randen A, et al. MRI and contrast-enhanced ultrasound imaging for evaluation of focal irreversible electroporation treatment: results from a phase I-II study in patients undergoing IRE followed by radical prostatectomy. Eur Radiol 2015; 26:2252–2260. [Crossref]
14. Vroomen LGPH, Scheffer HJ, Melenhorst MCAM, et al. MR and CT imaging characteristics and ablation zone volumetry of locally advanced pancreatic cancer treated with irreversible electroporation. Eur Radiol 2016; 27:2521–2531. [Crossref]
15. Barabasch A, Distelmaier M, Heil P, Krämer NA, Kuhl CK, Bruners P. Magnetic resonance imaging findings after percutaneous irreversible electroporation of liver metastases: a systematic longitudinal study. Invest Radiol 2016; 52:23–29. [Crossref]
16. Buijs M, van Lienden KP, Wagstaff PG, et al. Irreversible electroporation for the ablation of renal cell carcinoma: a prospective, human, in vivo study protocol (IDEAL Phase 2b). JMIR Res Protoc 2017; 6:e21. [Crossref]
17. Nielsen K, Scheffer HJ, Vieveen JM, et al. Anaesthetic management during open and percutaneous irreversible electroporation. Br J Anaesth 2014; 113:985–992. [Crossref]
18. Ljungberg B, Albiges L, Bensalah K, et al. EAU guidelines on renal cell carcinoma 2018. Euro Urol 2018; 29:451–458.
19. Monsky WL, Raptopoulos V, Keogan MT, et al. Reproducibility of linear tumor measurements using PACS: Comparison of caliper method with edge-tracing method. Eur Radiol 2004; 14:519–525. [Crossref]
20. McGraw KO, Wong SP. Forming inferences about some intraclass correlation coefficients. Psychol Methods 1996; 1:30–46. [Crossref]
21. Koo TK, Li MY. A guideline of selecting and reporting intraclass correlation coefficients for reliability research. J Chiropr Med 2016; 15:155–163. [Crossref]
22. Solomon SB, Silverman SG. Imaging in interventional oncology. Radiology 2010; 257:624–640. [Crossref]
23. Wendler JJ, Porsch M, Hühne S, et al. Short- and mid-term effects of irreversible electroporation on normal renal tissue: An animal model. Cardiovasc Intervent Radiol 2013; 36:512–520. [Crossref]

24. Deodhar A, Monette S, Single GW, et al. Renal tissue ablation with irreversible electroporation: Preliminary results in a porcine model. Urology 2011; 77:754–760. [Crossref]
25. Kingham TP, Karkar AM, D'Angelica MI, et al. Ablation of perivascular hepatic malignant tumors with irreversible electroporation. J Am Coll Surg 2012; 215:379–387. [Crossref]
26. Wagstaff PGK, de Bruin DM, van den Bos W, et al. Irreversible electroporation of the porcine kidney: Temperature development and distribution. Urol Oncol 2015; 33:168.e1–7. [Crossref]
27. Scheltema MJ, Postema AW, de Bruin DM, et al. Irreversible electroporation for the treatment of localized prostate cancer: A summary of imaging findings and treatment feedback. Diagn Interv Radiol 2017; 23:365–370. [Crossref]
28. Perzyna B, Stolzmann W. EAU guidelines on renal cell carcinoma. 2018; 29:451–458.

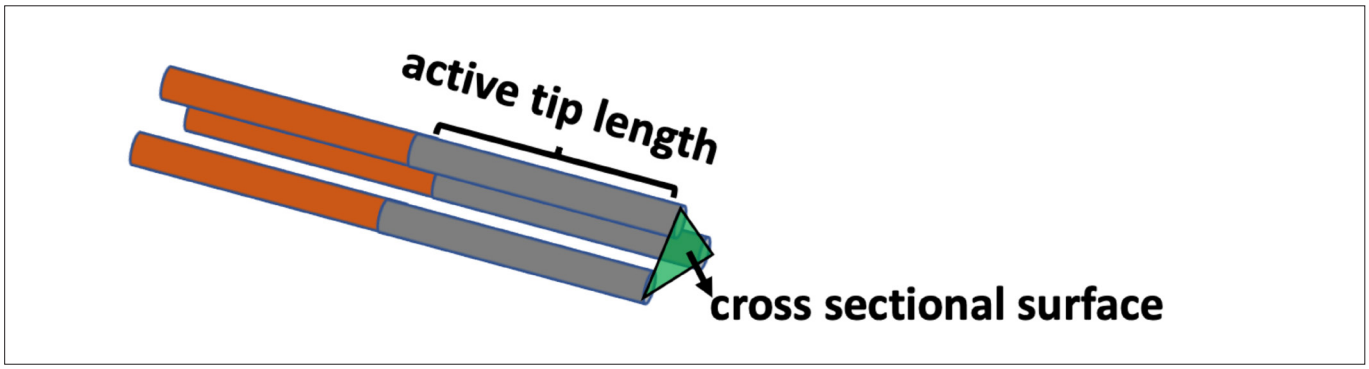

Supplementary Figure 1. The needle configuration volume is assessed prior to IRE ablation according to positioned needles. The cross-sectional surface between the IRE electrodes given by the software on the IRE console was multiplied by the active tip length to determine the volume.